Experimental study of the aerodynamic noise produced by flow-body interaction by synchronous PIV and microphone array measurements

Yoann Beausse, Vincent Valeau, Florent Margnat, Laurent-Emmanuel Brizzi, François Ollivier, Regis Marchiano

EXPERIMENTAL STUDY OF THE AERODYNAMIC NOISE PRODUCED BY FLOW-BODY INTERACTION BY SYNCHRONOUS PIV AND MICROPHONE ARRAY MEASUREMENTS

Y. Beausse[1] **V. Valeau**[1] **F. Margnat**[1]
L.-E. Brizzi[1] **F. Ollivier**[2] **R. Marchiano**[2]
[1] Institut PPrime - UPR 3346, CNRS-Université de Poitiers-ENSMA, France
[2] Institut Jean Le Rond d'Alembert - UMR 7190, Sorbonne Université, France
yoann.beausse@univ-poitiers.fr

ABSTRACT

The noise production of an air flow over a NACA 0012 airfoil is studied in an anechoic wind tunnel, especially the production of tonal noise at the trailing edge. The general goal of the study is to analyze jointly the velocity field along the spanwise direction and the acoustic far field. In this purpose, the velocity field is measured by using the Time-Resolved PIV technique (Particle Image Velocimetry at sampling frequency 20 kHz), while the radiated acoustic field is measured by a microphone array. The acoustic data are processed by using the beamforming technique, in the frequency domain. In the configuration studied here, the flow speed is set to 40m/s and the incidence of the airfoil is α=8° (parameters are chosen to generate tonal noise). The main result presented is the spatial distribution of the aeroacoustic sources in the spanwise direction. When multiple peaks are present in the acoustic far field spectrum, the beamforming analysis links each peak with a different source area along the trailing edge. This observation is coherent with a spectrum analysis of the PIV velocity field.

1. INTRODUCTION

The production of noise from flow-body interaction is a wide and fertile field of research. Its theoretical models are still discussed and improved, and have been well described by M. S. Howe (2002) [1]. In particular, this study will be focused on airfoil noise generation, which itself has long been a subject of interest, and previous experimental work can be found as soon as 1971 (Hersh & Hayden [2]). On the subject of tonal noise generation by an airfoil, the works of Paterson et al. (1973) [3] and Tam (1974) [4] have been very influential. Paterson first suggested an empirical model based on the vortex shedding, but Tam then argued that a feedback loop in the boundary layer better explained the results. The more recent work of Desquesnes, Terracol & Sagaut (2007) [5] presented a bidimensional numerical simulation of airfoil noise generation, and indicated a comb-shaped acoustic spectrum, with a main peak and secondary peaks separated with a constant frequency. These secondary peaks are shown to be dependent on a feedback loop between the main instability, which is the vortex shedding at the trailing edge, and the laminar separation bubble on the pressure side. The frequency of the main peak is linked to the most amplified Tollmien-Schlichting wave in the boundary layer, and the secondary peaks are explained by a periodic modulation of the amplitude of the main tonal frequency.

In order to track through experiments the mechanisms at the origin of the noise produced by the flow-body interaction, a Time-Resolved Particle Image Velocimetry (TR-PIV) measurement is chosen. The main interest of PIV over Hot-Wire Anemometry (HWA) is the absence of any intrusive probe in the flow, that could be responsible for radiated noise. However, the main problem of using PIV instead of a hot-wire in this purpose has for long been the insufficient sampling frequency, limited by the Laser and camera. For instance, Schröder et al. (2004) [6] investigated the trailing-edge noise with PIV in 2004, but they were limited to a sampling frequency of 4 kHz (while their microphone sampling frequency was 50 kHz).

A more recent study of the airfoil noise generation using PIV is the work of Pröbsting, Serpieri & Scarano (2014) [7], which revisits the work of Desquesnes et al. (2007) [5]. In this work, Pröbsting et al. use 6kHz PIV (in a plane perpendicular to the airfoil) to complement acoustic measurements, and find that in addition to the main vortex shedding responsible for the dominant tones, the scattering of vortical structures is also identified to be responsible for secondary tones. In the conclusion, the importance of spanwise coherence is reminded, and the validity of results of numerical studies based on 2D flow assumption (like the work of Desquesnes) is called into question.

Another method used in aeroacoustic analysis is the beamforming, which allows to locate acoustic sources by the use of an array of microphones. Like PIV, one of the main advantages of this technique is that it is non-intrusive. The method was very described by Dougherty [8] and Underbrink [9].

This experimental study especially focuses on the evolution of the aeroacoustic noise generation in the spanwise direction of the airfoil. The experimental apparatus is described in Section 2, first the facility used and then the methods employed in acoustic and PIV measurements. Afterwards some results of spectrum analysis are displayed in section 3, in which frequency beamforming and PIV anal-

ysis are also presented.

2. EXPERIMENTAL APPARATUS

2.1 Facility and Configuration

The experiment was conducted in the anechoic wind tunnel BETI (standing for *Bruit Environnement Transport Ingénierie*), located at the PPRIME Institute. The dimensions of the test section are 0.7 m (heigth) x 0.7 m (width) x 1.5 m (length). The walls, floor and ceiling around the open test section of the wind tunnel are covered with dihedral pieces of foam, insuring an anechoic behaviour for frequencies higher than 200 Hz.

To study the mechanisms behind the production of noise by flow-body interaction, a NACA 0012 airfoil is placed vertically in the middle of the test section. Its chord is $c = 200$ mm, and its wingspan is 890 mm (significantly more than the dimension of the flow : infinite wing configuration) and the flow speed is set to 40 m/s (with a precision of $\pm$ 0.1m/s). The Reynolds number based on chord and flow speed is 5.1 10^5. The incidence angle of the airfoil α is adjustable with a precision of half a degree (the axis of rotation is 9 cm downstream of the leading edge). In order to investigate different types of noise emission (tonal or broadband), a rough band is glued vertically on one side of the airfoil, 10 mm downstream of the leading edge (the rough band covers the whole wingspan and has a width of 15 mm). It was indeed noticed that with a non-zero incidence, the noise emitted is tonal if the rough band is on the suction side and becomes a broadband noise if the rough band is on the pressure side. The configuration chosen here is α = 8°, with the rough band on the suction side, as it is a standard tonal configuration.

2.2 Acoustic Measurements

The acoustic measurements of this study were made using the MegaMicros apparatus. MegaMicros is an array of microphones developed by Sorbonne University. The apparatus is specifically designed to perform beamforming analysis in the anechoic wind tunnel BETI, and can be seen assembled in BETI in Fig. 1.

The full array is composed of 4 identical planes, laid out around the flow in the shape of a quadrilateral frustum, but in this study only one of the planes is used. The plane holds 16 bars of 16 MEMS microphones (MicroElectro-Mechanical Systems), with the geometry presented in Fig.2, so the total number of microphones on the plane reaches 256. However, the design of the apparatus prevents the use of the lowest microphones (hidden behind a steel bar), and the final number of microphones used here is 208.

A plane is 1064 millimeters long in the streamwise direction and 1427 millimeters long in the spanwise direction, with a trapezoidal shape (see Fig. 2). The minimum distance between two microphones is 72 millimeters, ans the most distant microphones are 1.64 meters apart. More details on the MegaMicros apparatus can be found in the work of Zhou et al. (2020) [10, 11].

The sampling frequency of the array data is 50 kHz, and each measurement lasts for 10 s, for a total of 500000 points in time for each microphone.

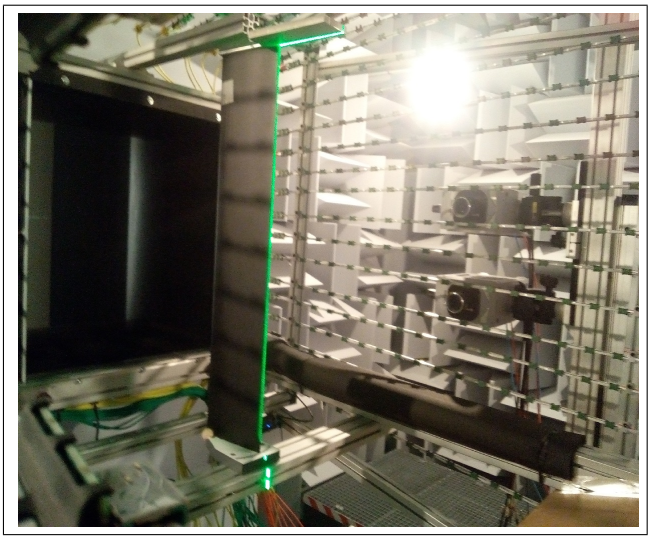

Figure 1. Photograph of the experimental apparatus. The flow comes from the convergent on the left of the image, and the Laser illuminates a vertical plane in the wake of the wing, from below. The two cameras used for PIV measurements can be seen behind the Megamicros plane used in this study.

2.3 PIV Measurements

Some PIV measurements were performed in the wake of the airfoil. The Laser illuminates a vertical plane, aligned with the airfoil to follow the deviation of the flow when the incidence is non-zero. The laser sheet thickness is estimated to be around 2 mm. Two high-speed cameras are placed one above the other, and each one records a 304x304 mm image, composed of 1024x1024 pixels (3.4 pxls/mm). The upper part of the image recorded by the camera underneath is the same as the lower part of the image recorded by the camera above. This overlap is 10 mm wide.

In the PIV algorithm, the interrogation window size comes from 64x64 pixels to a minimum of 16x16 pixels, so each vector on the final velocity field will be spaced out by 8 pixels, which is here equivalent to 2.4 mm. The PIV measurements carried out in this study are set in Time-Series Mode (TSM), meaning that a velocity profile is calculated between each image and its successor.

A final sketch of the entirety of the apparatus is presented in Fig. 3, in which the geometric scales are respected.

3. RESULTS

3.1 Acoustic Results

As stated in part 2.1, the flow (U_∞=40m/s) over a NACA 0012 (chord c = 200mm) is studied, with an angle of inci-

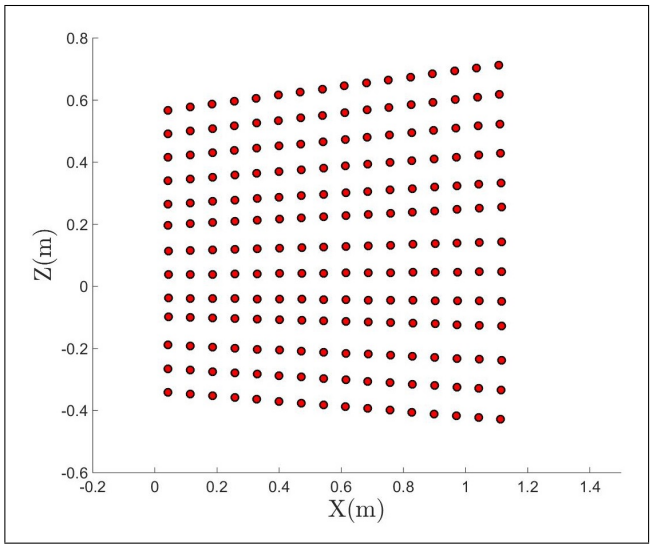

Figure 2. Representation of a plane of the MegaMicros array. On the axes, distances in meters, X being the streamwise direction and Z the spanwise direction. The microphones are attached to 13 aluminium bars along the X direction.

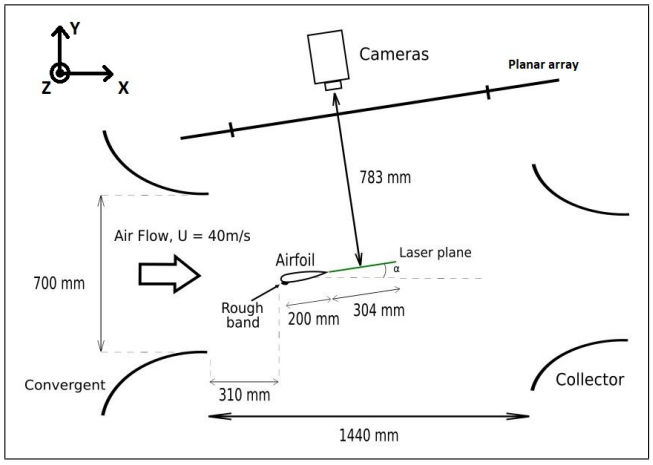

Figure 3. Sketch of the experimental apparatus.

dence $\alpha = 8°$. The Reynolds number based on the chord is 5.1 10^5.

The far field acoustic spectra are calculated using the Welch's method. An acoustic measurement contains 500000 points per channel (10s of signal sampled at 50 kHz), and this data is divided in sets of 4096 points for the Welch's method. The frequency resolution is 12.2 Hz, and the final result is the average of 122 spectra. The Power Spectrum Densities (PSD) are plotted in dB SPL ($P_{\text{ref}} = 2.10^{-5}$ Pa).

Fig. 4 presents the PSD of the signal of a single microphone of the array (all spectra are very similar). Over the global decrease due to the turbulent energy cascade, a comb-shape with 3 main peaks emerges, at f_1=1600 Hz, f_2=1710 Hz (the highest peak) and f_3=1900 Hz. The second and third harmonics of these peaks (with the same shape, only smaller) also appear.

As this configuration was specifically chosen to generate tonal noise, the presence of a major peak is expected. This frequency is most probably the characteristic frequency of the vortex shedding in the wake of the airfoil, as was already clearly established by Pröbsting et al. [7]. The secondary peaks noticed by Desquesnes et al. [5] (in numerical simulations) are present. They were analyzed as the result of a feedback loop between the vortex shedding at the trailing edge and the laminar separation bubble on the pressure side.

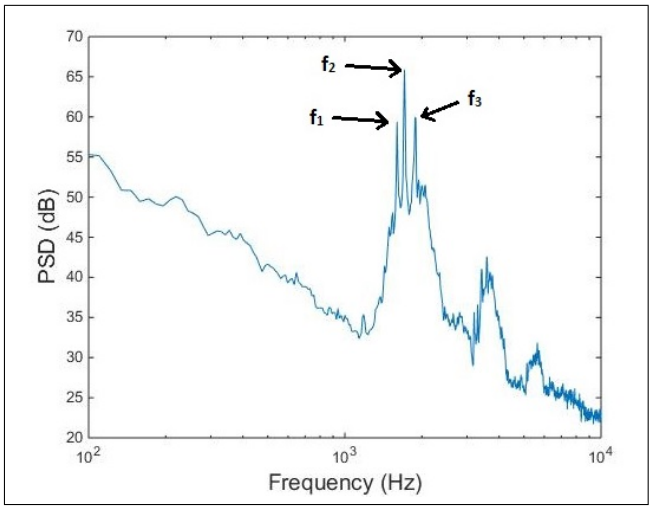

Figure 4. PSD of the acoustic far field signal, in tonal noise configuration (α=8°, Re=5.1 10^5). The three main peaks are indicated at f_1=1600 Hz, f_2=1710 Hz (highest peak) and f_3=1900 Hz.

3.2 Beamforming Results

The conventional frequency-domain beamforming algorithm is applied to the array data. The beamforming technique requires the calculation of the Cross-Spectral Matrix (CSM). Each element of this matrix is computed by using Welch's method, with the same parameters as for the PSD presented above. Each beamforming map is computed in a band of 100 Hz centered on a given frequency.

In order to take into account the presence of the flow when computing the travel times for the acoustic waves, a shear flow correction has been implemented, based on the work of Amiet [12]. The CLEAN-SC algorithm developed by Sijtsma [13] is also used to refine the beamforming maps.

The beamforming maps in Fig. 5 are obtained when focusing on the airfoil plane and first confirm that for this configuration, at the three main peaks of acoustic emission, the source of noise is located at the trailing edge of the airfoil. However, it is also clearly shown that the exact location in the spanwise dimension of the acoustic source depends on frequency : each frequency peak is not distributed along the span but emitted at a different location on the trailing edge. This three-dimensional aspect did not appear in the work of Desquesnes et al. [5] (bidimensional analysis, strong coherence in the spanwise direction is assumed) or Pröbsting et al. [7] (yet they expressed caution

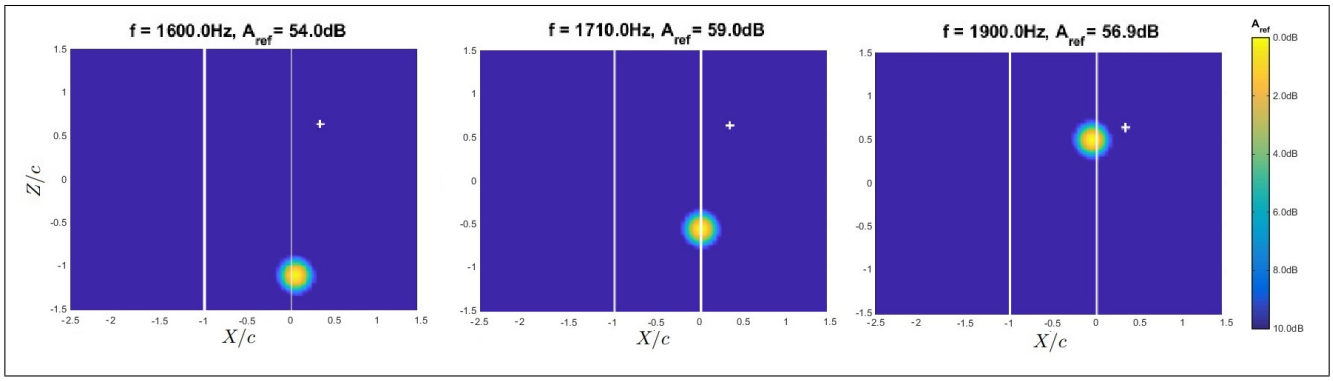

Figure 5. Frequency-domain beamforming maps, for frequencies f_1=1600 Hz, f_2=1710 Hz and f_3=1900 Hz (peak frequencies of Fig. 4). White lines represent the position of the airfoil (as the tips are out of the image, only the leading edge in X/c = -1 and the trailing edge in X/c = 0 can be seen). For each subfigure, A_{ref} denotes the maximum level of the soundmap in dB.

in considering this 2D flow assumption).

3.3 PIV Results

First, the consistency of the spanwise profile of the mean velocity $\bar{U}$ close to the trailing edge (at $X/c = 0.25$) is assessed. Fig. 6 shows that the maximum variability around the average value of $\bar{U}$ is inferior to 5 %; the homogeneity of the mean flow field in the spanwise direction is satisfactory.

The spanwise distribution of the fluctuating velocity is also investigated in Fig. 7, by calculating the root mean square U'_{rms} of the velocity fluctuations at $X/c = 0.25$. The peak around $Z/c = 0$ is in all likelihood explained by the fact that (like already stated in Part 2.3) in the middle of the image, both cameras are filming. In this overlap zone, the velocity is computed twice and then averaged, which could explain the loss of turbulence intensity. On the upper and lower part of the image ($Z/c > 1.2$ and $Z/c < -1.2$), the turbulence is also more important. Outside of these particular zones, the turbulence fluctuates moderately, U'_{rms} staying between 80% and 110% of its mean value.

Fig. 8 presents a snapshot of the velocity fields. Vortical structures are shed from the trailing edge, and convected downstream. These structures decay gradually and are less visible for values of X/c higher than 1.

In order to investigate the evolution of the velocity fluctuations in the spanwise direction Z, the velocity spectrum is computed at each point in this direction ($\Delta Z/c = 0.012$ between adjacent points), along the line X/c = 0.25. The Welch method is used again, and the spectrum is calculated using the same number of points (4096), but here, the number of averages is 10 and the frequency resolution is 5 Hz. This is due to the changes in sampling frequency (20 kHz in PIV instead of 50 kHz for the array of microphones) and in duration of the signal (2 seconds instead of 10). The result is then normalized by $\rho {U_\infty}^2$, ρ being the average density of air (1.2 kg/m^3) and U_∞ the incoming flow speed (40 m/s).

Fig.9 shows a spatial differentiation, in the spanwise direction : three zones can be delimited. For values of Z/c between -1.4 and -0.6, the main frequency is f_1=1600 Hz. Between -0.6 and 0, the main frequency is f_2=1715 Hz, and for Z/c between 0 and 1, it is f_3=1880Hz. This behaviour is very similar to the one already seen in Fig. 5, with acoustic sources.

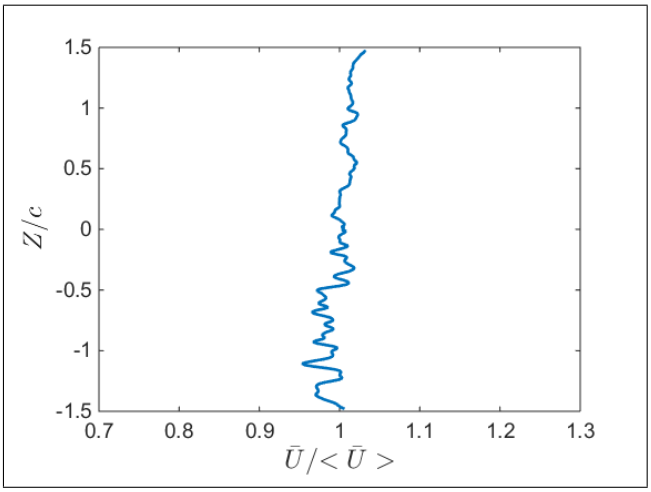

Figure 6. Normalized mean velocity profile $\bar{U}/ < \bar{U} >$ along the spanwise direction Z, in the wake of the NACA 0012 at $X/c = 0.25$. $\bar{U}$ is the local time average of the velocity at each point, and $< \bar{U} >$ is the average of $\bar{U}$ along the whole line $X/c = 0.25$.

The velocity spectrum is then plotted for specific values of Z/c, in order to better investigate the fluctuations around the main peak. On Fig. 10 (which corresponds to the situation in the middle section), the three peaks (for f_1, f_2 and f_3) are present, and the main frequency is f_2, like in the acoustic far field spectrum. On contrary, on Fig. 11, only the main peak in this area (f=f_3) is visible. It is then concluded that the vortices detaching from the trailing edge are not homogeneous along the span of the airfoil (probably due to flow conditions that are not perfectly uniform along the Z direction), which produce significant local changes of the sound source along the span.

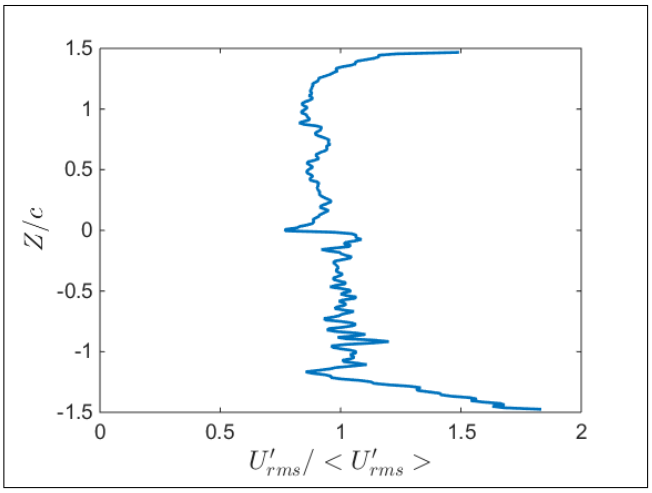

Figure 7. Distribution of the normalized fluctuating velocity $U'_{rms}/ < U'_{rms} >$ along the spanwise direction, in the wake of the NACA 0012 at $X/c = 0.25$. U'_{rms} is the local root mean square of the velocity fluctuations, and $< U'_{rms} >$ is the average of U'_{rms} along the whole line $X/c = 0.25$.

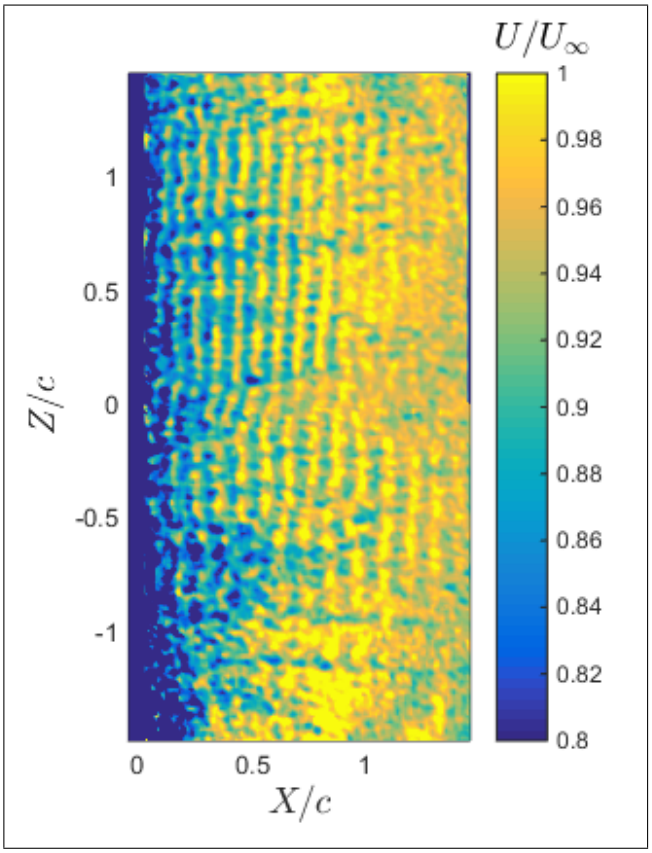

Figure 8. Instantaneous velocity field in the wake of a NACA 0012 airfoil as a function of X/c (streamwise direction) and Z/c (spanwise dimension). $X/c = 0$ corresponds to the trailing edge.

4. CONCLUSION

The generation of tonal noise on the trailing edge of a NACA 0012 airfoil has been studied. As was previously seen in preceding works, this noise (which only appears on certain configurations) is constituted of multiple discrete peaks. The main originality of this study is the spatial analysis of the acoustic source in the spanwise direction. Using a frequency domain beamforming analysis, it was observed that different frequencies are associated with different source regions along the trailing edge. In the case studied here, three regions were identified, each one linked with a peak in the acoustic spectrum. Moreover, TR-PIV measurements were carried out, and the same phenomenon appears when investigating the velocity spectra in the wake of the airfoil. The same three zones are again clearly identified. As was stated in the work of Pröbsting et al. [7], this emphasizes on the importance of considering spanwise variations while analyzing this phenomenon, and questions the validity of explanatory models developed with a bidimensional hypothesis.

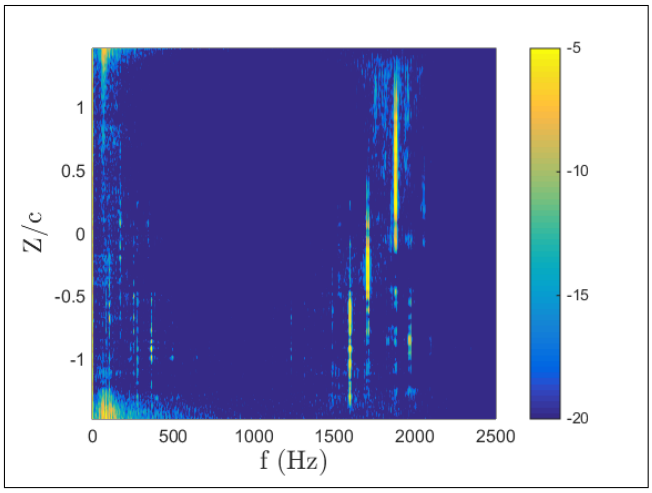

Figure 9. Velocity PSD as a function of Z/c (spanwise dimension) and frequency (in Hz), at $X/c = 0.25$. Power spectral density is plotted in dB, with $\rho {U_\infty}^2$ taken as reference.

5. ACKNOWLEDGEMENTS

The authors warmly acknowledge Romain Bellanger, Pascal Biais, Patrick Braud, Janick Laumonier, Laurent Philippon and Jean-Christophe Vergez for their invaluable technical support. This work is supported by Région Nouvelle Aquitaine and Agence Nationale de la Recherche (ANR).

6. REFERENCES

[1] M. S. Howe. *Theory of Vortex Sound*. Cambridge University Press, 2002.

[2] A. S. Hersh, R. E. Hayden. Aerodynamic sound radiation from lifting surfaces with and without leading-edge serrations. NASA *Tech. Rep.* 114370, 1971.

[3] Robert W. Paterson, Paul G. Vogt, Martin R. Fink and C. Lee Munch. Vortex noise of isolated airfoils *J. of Aircraft*, *vol. 10, No. 5*, 1973.

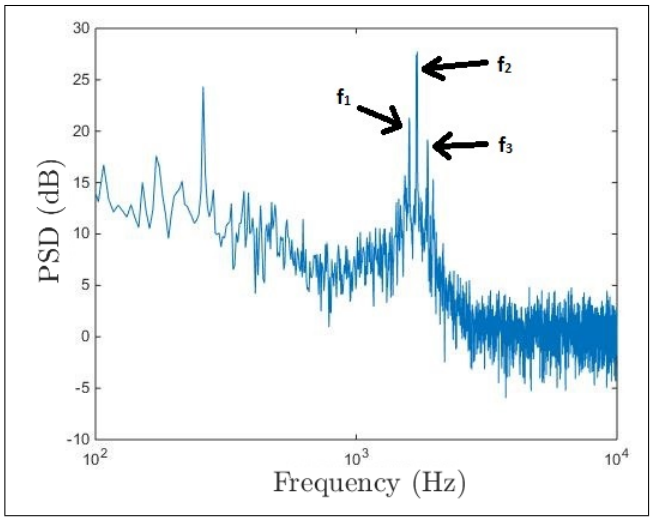

Figure 10. Velocity PSD as a function of frequency (in Hz), at the point $(X/c = 0.25; Z/c = -0.5)$. f_1=1600 Hz, f_2=1715 Hz and f_3=1880 Hz. Power spectral density is plotted in dB, with $\rho {U_\infty}^2$ taken as reference.

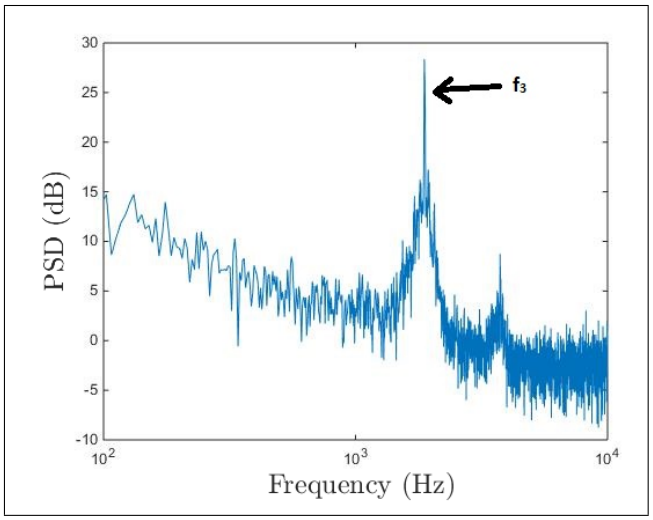

Figure 11. Velocity PSD as a function of frequency (in Hz), at the point $(X/c = 0.25; Z/c = 0.5)$. f_3=1880 Hz. Power spectral density is plotted in dB, with $\rho {U_\infty}^2$ taken as reference.

[4] C. K. W. Tam Discrete tones of isolated airfoils *J. Acoust. Soc. Am.*, *Vol. 55, No. 6*, 1974.

[5] G. Desquesnes, M. Terracol and P. Sagaut. Numerical investigation of the tone noise mechanism over laminar airfoils. *J. Fluid Mech.*, *vol.591*:155–182, 2007.

[6] A. Schröder, U. Dierksheide, J. Wolf, M. Herr and J. Kompenhans. Investigation on trailing-edge noise sources by means of high-speed PIV *12th Int Symp on Applications of Laser Techniques to Fluid Mechanics*, Lisbon, Portugal, July 12-15 2004

[7] S. Pröbsting, J. Serpieri, and F. Scarano. Experimental investigation of aerofoil tonal noise generation. *J. Fluid Mech.*, *vol.747*:656–687, 2014.

[8] Robert P. Dougherty Beamforming in acoustic testing. *Aeroacoustic Measurements* (Thomas J. Mueller, Springer), chap. 2, 2002

[9] James R. Underbrink Aeroacoustic phased array testing in low speed wind tunnels. *Aeroacoustic Measurements* (Thomas J. Mueller, Springer), chap. 3, 2002

[10] Y. Zhou, F. Ollivier, P. Challande, R. Marchiano, V. Valeau, D. Marx, C. Prax. Design and use of a three-dimensional array of MEMS microphones for aeroacoustic measurements in wind-tunnels. In *Berlin Beamforming Conference*, 2020.

[11] Y. Zhou, V. Valeau, J. Marchal F. Ollivier, R. Marchiano. Three-dimensional identification of flow-induced noise sources with a tunnel-shaped array of MEMS microphones. *J. Sound and Vibration.*, *vol.482*:155–182, 2020.

[12] Amiet, R. Correction of open jet wind tunnel measurements for shear layer refraction 2nd Aeroacoustics Conference, 1975, 532

[13] Sijtsma, P. CLEAN based on spatial source coherence Int. J. Aeroacoustics, SAGE Publications Sage UK: London, England, 2007, 6, 357-374